

# Simulation of 2D ballistic deposition of porous nanostructured thin-films

S. Bukkuru<sup>a,\*</sup>, H. Hemani<sup>b</sup>, S. M. Haque<sup>c</sup>, J. Alphonsa<sup>a</sup>, K. Divakar Rao<sup>c,d</sup>, M. Warriar<sup>b,d</sup>

<sup>a</sup>Facilitation Centre for Industrial Plasma Technologies, IPR, Gandhinagar, Gujarat, India - 382 016

<sup>b</sup>Computational Analysis Division, BARC, Visakhapatnam, Andhra Pradesh, India - 531 011

<sup>c</sup>Atomic & Molecular Physics Division, BARC, Visakhapatnam, India - 531 011

<sup>d</sup>Homi Bhabha National Institute, Anushaktinagar, Mumbai, Maharashtra, India - 400 094

---

## Abstract

A “two-dimensional ballistic deposition” (2D-BD) code has been developed to study the geometric effects in ballistic deposition of thin-film growth. Circular discs are used as depositing specie to understand the shadowing effects during the evolution of a thin-film. We carried out the 2D-BD simulations for the angles of deposition 20°–80° in steps of 10°. Standard deviations 1°, 2°, 4°, 6° and 10° are used for each angle of deposition with disc size of 1.5 Å to understand its effect on the microstructure of the thin-films. Angle of growth, porosity and surface roughness properties have been studied for the afore-mentioned angles of deposition and their standard deviations. Ballistic deposition simulations with the discs of different sizes have been carried out to understand the effect of size in ballistic deposition. The results from this code are compared with the available theoretical and experimental results. The code is used to simulate a collimated glancing angle deposition (C-GLAD) experiment. We obtain a good qualitative match for various features of the deposits.

*Keywords:* Thin-film, ballistic deposition, glancing angle, simulation

---

## 1. Introduction

Vapor deposition is one of the most preferred techniques for the fabrication of high-purity and high-performance thin-films which have a broad spectrum of applications [1]. In this technique, the vapour of a material to be coated is deposited on a substrate through condensation. If the precursor vapour is produced from a physical process, it is called physical vapour deposition (PVD) and alternatively, if the precursor

---

\*Corresponding author

*Email addresses:* srinivasaraobukkuru@gmail.com (S. Bukkuru), harshscience777@gmail.com (H. Hemani), maidul@barc.gov.in (S. M. Haque), alphonsa@ipr.res.in (J. Alphonsa), divakar@barc.gov.in (K. Divakar Rao), manoj.warrier@gmail.com (M. Warriar)

vapour is produced from a chemical process, it is called chemical vapour deposition (CVD). Historically, PVD was reported more than 150 years ago by W.R. Grove in 1852 [2] and M. Faraday in 1857 [3]. However, a great variety of applications of vapour deposition technique have been witnessed in the past few decades. [1, 4, 5]. This became possible with the advancement of its subclasses such as “Oblique Angle Deposition (OAD)”, “GLancing Angle Deposition (GLAD)”, etc. OAD is performed typically with a fixed, obliquely inclined substrate to the incoming flux of depositing particles. Whereas in GLAD, which is an extension of OAD, the substrate undergoes individual or combined effects of change in relative position, inclination or rotation [6].

The early research in the thin-film deposition was primarily experimental. The pioneering simulations of ballistic deposition by Vold and Sutherland [7, 8] describe the sedimentation and aggregation in collides. This developed considerable interest in simple ballistic deposition simulations to understand the critical growth mechanisms and for predicting the thin-film morphologies [9, 10, 11, 12, 13, 14, 15]. In ballistic deposition (BD), depositing particles are represented by hard particles projected towards a substrate in selected angular distribution. These particles are projected one after the other and travel linearly until they reach the substrate, or, are intercepted by previously deposited particle(s). The particle is always assumed to remain in contact with the particle(s) with which it makes the first contact. The capture length of particles arriving later will be reduced by the particles that have previously been deposited giving rise to a “shadowing effect” [9, 11]. With this, symmetric impingement of a projected particle is no longer possible about the centre of previously deposited particle and hence their mean pair orientation shifts towards the normal resulting in the reduction of the angle of growth ( $\beta$ ) than the angle of deposition ( $\alpha$ ) [11].

The initial study of the ballistic deposition simulations of Henderson et al. [9] provides details about the columnar growth morphology. However, they obtained lesser densities as compared to the experimental results. In a subsequent study, they used an “atomic relaxation” scheme of the projected particle in which they tuned the extent of relaxation to match with experimental densities [10]. Dirks et al. [11] used Henderson’s model and obtained thin-film structures which are morphologically similar to experimentally obtained morphologies with and without the limited atomic relaxation. Moreover, Dirks et al. [11] have shown that the atomic relaxation scheme of Henderson et al. can lead to the formation of hexagonal crystallites and random close packing structures in two and three dimensions respectively, which are not observed in experiments. Therefore BD models are used to reproduce the morphological characteristics of thin-films with limited atomic relaxation or without relaxation.

Meakin has carried out extensive 2D and 3D simulations of ballistic deposition and found that a simple

2D ballistic deposition model reproduces the columnar morphology with limited relaxation [16]. In light of the above studies, it seems worthwhile to use a two dimensional ballistic deposition model to study the formation of nano-structures in glancing angle deposition experiments. We would like to address the issue of lesser densities observed by Henderson et al. [9] with the “size of the discs” instead of the “atomic relaxation”. We would also like to apply the concept of this simple ballistic deposition to a collimated glancing angle deposition (C-GLAD) experiment carried out by Haque et al. [17] which helps in predicting the results of future experiments of this kind.

In the present study, we developed a “two-dimensional ballistic deposition (2D-BD)” code to study the geometric effects of thin-film growth. This code is described in Section 2. We carried out 2D-BD simulations to study the angle of growth, porosity, RMS surface roughness as a function of the angle of deposition. In total, 119 simulations have been analysed to understand the geometric effects in thin-film growth. The results obtained from 2D-BD simulations have been compared with the results from the available theoretical and experimental results for validation and are described in Section 3. The 2D-BD code is then applied to the collimated glancing angle deposition (C-GLAD) experiment conducted by Haque et al. [17]. The results for this are presented in Section 4. Finally, the conclusions are summarized in Section 5.

## **2. 2D Ballistic Deposition – Method**

A “two-dimensional ballistic deposition” (2D-BD) code has been developed to study the geometric effects of thin-film growth. We consider discs with a fixed radius to represent particles. The particles to be deposited, are initialized on a straight line which maps the source to the target using a uniform random number generator as shown in Figure 1. The particles are launched along the chosen angle of deposition using a normal angular distribution. This lets us specify a standard deviation for the angle of deposition. The projected particle at a given angle of deposition travels rectilinearly from the source to the substrate and gets deposited. If the launched particle is intercepted by an earlier particle that was deposited on the substrate, it sticks to the particle. If it meets more than one particle simultaneously, it sticks with them. Periodic boundary conditions are applied at the edges of the substrate. In the present study, we deliberately do not consider the “bouncing” or “atomic relaxation” after the projected particle makes its first contact, since the morphology is not significantly affected with or without limited atomic relaxation [11]. This study is focused on geometry-based shadowing effects in the thin-film evolution and comparison of such a model with experimental results.

2D-BD simulations have been carried out for the angles of deposition  $20^\circ$  -  $80^\circ$  in steps of  $10^\circ$  with the

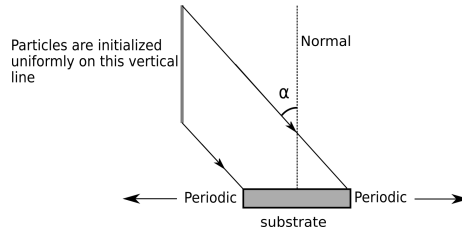


Figure 1: Schematic diagram of ballistic deposition. Particles are initialized uniformly from a vertical line and launched towards the substrate at a given angle of deposition.

normal distribution. Standard deviations of  $1^\circ$ ,  $2^\circ$ ,  $4^\circ$ ,  $6^\circ$ ,  $10^\circ$  are used for the above-mentioned angles of deposition to study its effect on film growth. In each simulation, one million particles with a fixed radius have been projected on to a substrate of length one micron. To understand the effect of size of particles, simulations with particles of radius  $1.0 \text{ \AA}$ ,  $1.5 \text{ \AA}$ ,  $2.0 \text{ \AA}$  and  $2.5 \text{ \AA}$  have been carried out for the above-mentioned angles of deposition using a standard deviation of  $1^\circ$ . Furthermore, since the growth is a random process, ten trials of simulations have been carried out for each of these angles of deposition with a standard deviation ( $1^\circ$ ) and disc radius of  $1.5 \text{ \AA}$ . The typical height of most of the grown films are  $\approx 200 \text{ nm}$ . In total, 119 simulations have been analysed to understand the geometric effects of thin-film growth. Typically, a  $200 \text{ nm}$  2D film can be grown on  $1000 \text{ nm}$  substrate on a standard laptop in 10 hours.

The results from this code are compared with the available theoretical and experimental results in Section 3. Apart from the afore-mentioned simulations, we also carried out 2D-BD simulations for investigation of a collimated glancing angle deposition (C-GLAD) experiment by Haque et al. [17] and the results are presented in Section 4.

### 3. Results and Discussion

The results are presented and discussed below in the following Subsections 3.1–3.3.

#### 3.1. Angle of growth of thin-film

Much of the earlier work concentrated on the “tilted column morphology” and the relationship between the angle of deposition ( $\alpha$ ) and the angle of growth ( $\beta$ ) of the thin-films. With simple geometric effects, the earlier two-dimensional ballistic deposition simulations could reproduce several key observations such as  $\beta < \alpha$  and monotonic decrease in the density of thin-film with the increase in the angle of deposition [9]. Various rules have been proposed to describe the relationship between the angle of deposition ( $\alpha$ ) and the

angle of growth ( $\beta$ ). We compare our results for the angle of growth as a function of the angle of deposition with two widely used empirical models described below.

The “tangent rule” was developed by Nieuwenhuizen and Haanstra [18] by empirically fitting their experimental data (Eq. 1).

$$\tan\alpha = 2 \tan\beta \quad \text{or} \quad \beta = \tan^{-1}(0.5 \tan\alpha) \quad (1)$$

It was later modified by Hodgkinson et al. [19] by adding a fitting parameter ( $k$ ), which depends on the material (Eq. 2).

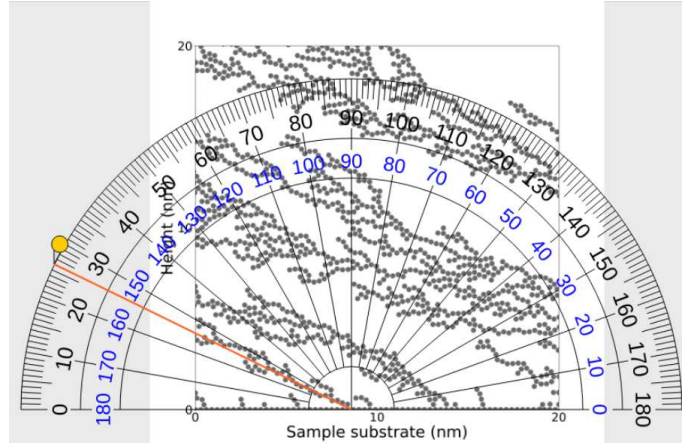
$$\beta = \tan^{-1}(k \times \tan\alpha) \quad \text{and} \quad k < 0.5 \quad (2)$$

Tait et al. [20] derived the “cosine rule” using a ballistic deposition model (Eq. 3).

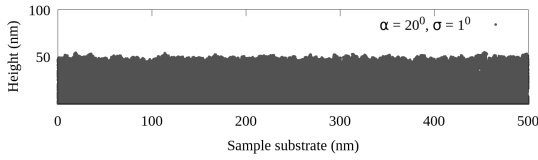
$$\beta = \alpha - \arcsin\left(\frac{1 - \cos\alpha}{2}\right) \quad (3)$$

We have observed the earlier reported “tree-like structures” at the atomistic scales [11, 16, 15] in all the simulations for all the angles deposition carried out in the present study as seen in Figure.2a. The height of these structures increases with deposition. The branching in tree-like structures is more and they are more closely packed at smaller angles of deposition ( $20^\circ$ ,  $30^\circ$ ). Therefore for these angles, a thin-film looks continuous as shown in Figure 2b. The shadowing effects in a ballistic deposition, increase with the increase in the angle of deposition. With the increasing shadowing effects, there is more space between the ‘tree-like structures. One can see these structures as closely spaced, thin, tilted columns for the angles of deposition  $40^\circ$ ,  $50^\circ$ . The size and space between these tilted columns increase with the angle of deposition and also with the standard deviation. The tilted columns are easily discerned for the angles of deposition  $\geq 60^\circ$ . Figure 2c shows the tilted columns formed at an angle of deposition  $80^\circ$  with a standard deviation of  $1^\circ$ .

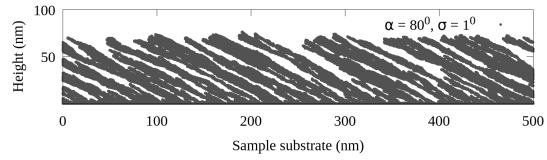
The tilted columns of a thin-film are mostly parallel to each other. The angle of growth of these tilted columns is considered to be the angle of growth of the thin-film. Few columns may not be parallel to the remaining due to “column extinction” at some points due to shadowing effects. The height and orientation of any specific column depend on the orientation and height of the adjacent shadowing columns. In the present study, this issue is taken care by considering an average value of angles of many tilted columns for each simulation. Further, at each angle of deposition with a standard deviation of  $1^\circ$ , ten simulations with different random number seeds are carried out. The angle of growth from these ten simulations are obtained as described above and their average value is considered. These angles of growth and their standard



(a) Atomistic view of tilted columns formed at an angle of deposition of  $80^\circ$  with a standard deviation of  $1^\circ$ . Here, the angle of growth is  $64^\circ$  from the normal.



(b) Here the angle of deposition is  $20^\circ$  with a standard deviation of  $1^\circ$  and the angle of growth is  $17^\circ$



(c) Here the angle of deposition is  $80^\circ$  with a standard deviation of  $1^\circ$  and the angle of growth is  $64^\circ$ .

Figure 2: (a) A zoomed in figure of tree-like structures of connected particles from the simulations are shown. (b) Smaller angles of deposition result in frequent branching and lesser spacing between these structures and thus the films appear continuous. (c) The space between these patterns increases with the increase in the angle of deposition. For deposition angles  $\geq 60^\circ$  the structures are discernable.

deviations are estimated and compared with the available theoretical and experimental results in Figure 3. The angle of growth increases with the angle of deposition. The values of angle of growth are also estimated at each angle of deposition with standard deviations of  $1^\circ$ ,  $2^\circ$ ,  $4^\circ$ ,  $6^\circ$ ,  $10^\circ$  to understand the effect of standard deviation in the angle of deposition. It is found that there is no significant change in the angle of growth with the change in standard deviation for a particular angle of deposition.

Figure 3 shows the relationship between the angle of deposition and the angle of growth obtained from the simulations as described above and compares it with the empirical rules [18, 20] and experiments [21, 22, 23, 24]. The mean values of angles of growth from the simulations lie in between the values estimated by tangent and cosine rules. They are found to match closely with the experimental results [22, 24] for pure metals. For the metal oxides, a qualitative match is seen, but quantitatively the simulation shows higher values for the angle of growth. Meakin et al. extensively studied the large scale numerical simulations of lattice and off-lattice growth models using ballistic deposition, fractal scaling and several other aspects for

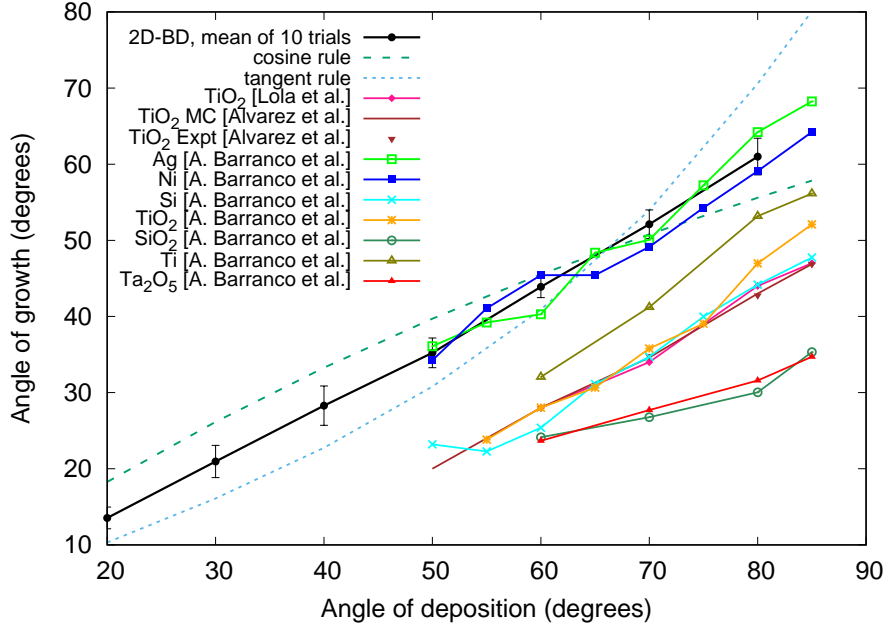


Figure 3: The angle of growth increases with the angle of deposition. The mean values of angle of growth are estimated for ten trials at each angle of deposition from 20°–80° with a standard deviation of 1° using circular discs of radius 1.5 Å.

about two decades using 2D and 3D off lattice ballistic deposition models ([25, 26, 27, 28, 29, 30, 31]). The angle of growth values from our simulations match the 2D and 3D simulations by Meakin et al [29] within a range of 1–3°.

Though there is no significant change in the angle of growth with the change in the standard deviation, there are morphological changes like shape of the thin-film deposition, thickness of tilted columns. Figure 4 shows the increase in the thickness of tilted columns with an increase in the standard deviation. This figure qualitatively supports the earlier reported power law of columns ( $w \sim d^{p'}$ ), i.e. the width ( $w$ ) of a column increases with its length ( $d$ ). Here  $p'$  is the growth exponent and its value is 0.5 [32]. Mukherjee et al. reported that this value drops to a lower value than 0.5 when surface diffusion also plays a role beyond a critical value,  $\theta_c = 0.24 \pm 0.02$  from their two-dimensional analytical model [33]. Here  $\theta_c = T_s/T_m$  where  $T_s$  is the substrate temperature and  $T_m$  is its melting point. The present ballistic deposition code, 2D-BD does not consider the surface diffusion and it is applicable below the critical temperature where surface diffusion has no significant role.

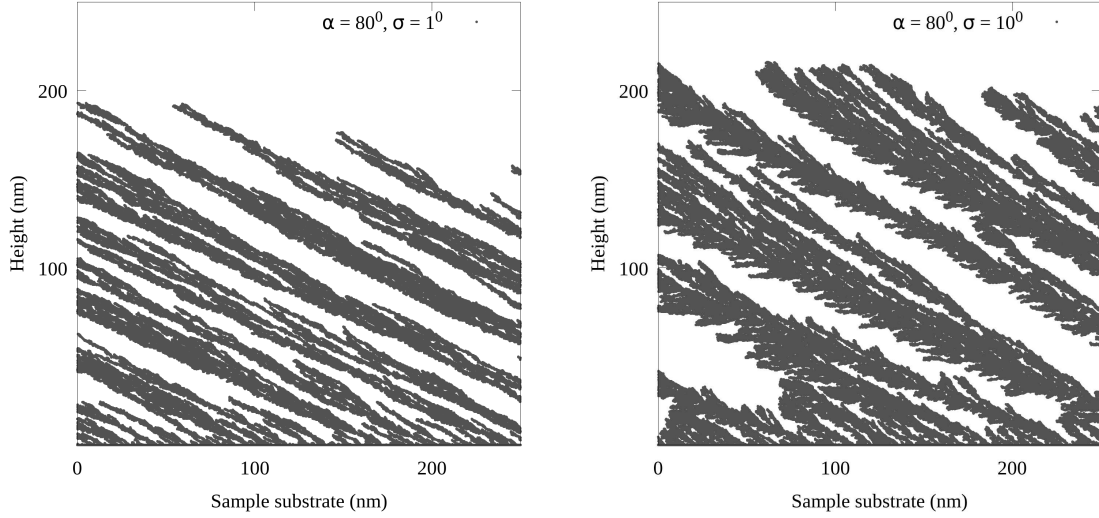


Figure 4: For a particular angle of deposition, angle of growth remains constant with the increase in standard deviation, but the width of tilted columns increases.

### 3.2. Porosity

Porous thin-films have a broad spectrum of applications due to their adequate characteristics such as high resistance to thermal shock, low thermal conductivity, etc. Using oblique angle deposition (OAD), one can engineer the required porosity for various applications. In two-dimension:

$$Porosity = \frac{Void\ area}{Total\ area} = \frac{Total\ area - Area\ occupied\ by\ discs}{Total\ area} \quad (4)$$

Porosity (P) increases with the angle of deposition [34, 23, 35, 36] and remains constant with the height of the film [37]. Figure 5 shows the porosity (P) as a function of angle of deposition ( $\alpha$ ) and confirms that porosity increases with the increase in the angle of deposition. It can also be seen that porosity increases with an increase in the radius (r) of the particle used in the simulation, which is a geometric effect. The effect of standard deviation ( $\sigma$ ) is found to be insignificant at any specific angle of deposition ( $\alpha$ ). Earlier, Sood et al. have used the following expression (5) with a fitting parameter  $c$  to fit their experimental results with their Monte Carlo simulations for indium tin oxide (ITO) [35].

$$P = \frac{\theta \tan \theta}{c + \theta \tan \theta} \quad \text{Where } c = 8.32 \text{ and } \theta \text{ is the angle of deposition.} \quad (5)$$

The results for porosity, reported in the present study, follow the trend observed in experiments. In most of the earlier theoretical studies of ballistic deposition, scaling behaviour of porosity is studied using the

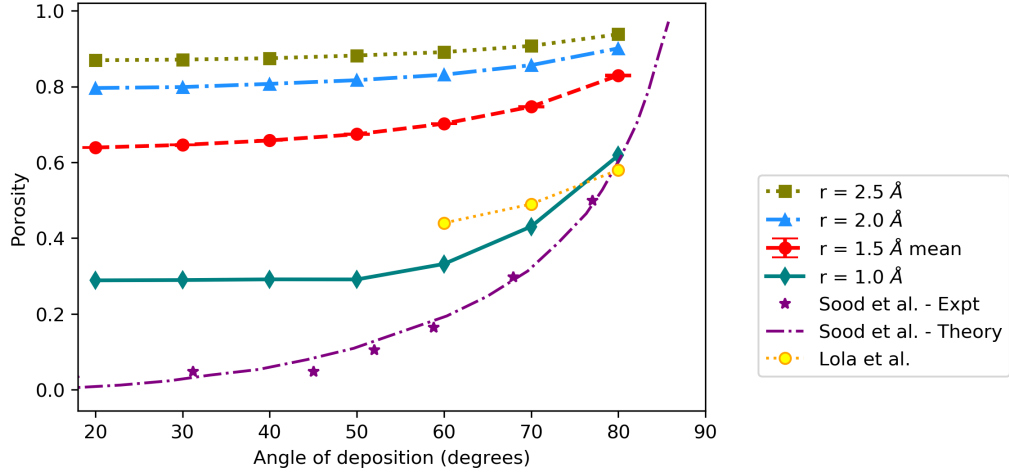


Figure 5: Porosity increases with the angle of deposition and also with the radius ( $r$ ) of the particles.

particles with unit size, with different sticking probabilities or with the relaxation of particles [10, 14, 38, 39, 40, 41]. To the best of our knowledge the effect of size of particles on the porosity has not been reported. Here, it is suggested that in simulations, one needs to use the discs of size comparable to that of particles of practical interest, for a quantitative match with the experimental results.

### 3.3. RMS Surface Roughness

Roughness is defined as how the height ( $h(r)$ ) of a surface deviates from its average height ( $\bar{h}$ ). It is measured by finding the root mean square (RMS) variation of the height and is expressed by the interface-width  $w(L)$  [42] as shown below (Eq. 6).

$$w(L) = \sqrt{\frac{1}{L^2} \Sigma [h(r) - \bar{h}]^2} \quad (6)$$

where  $L$  is the linear size of the surface and  $\bar{h}$  is given by the following expression (Eq. 7).

$$\bar{h} = \frac{1}{L^2} h(r) \quad (7)$$

However, in the present simulations, the roughness is measured using the following expression similar to [43] as:

$$R_q = \sqrt{\frac{\Sigma_{i=1}^N (h_i - \bar{h})^2}{N}} \quad (8)$$

Here, mean height ( $\bar{h}$ ) is estimated for the sampling length of the substrate.

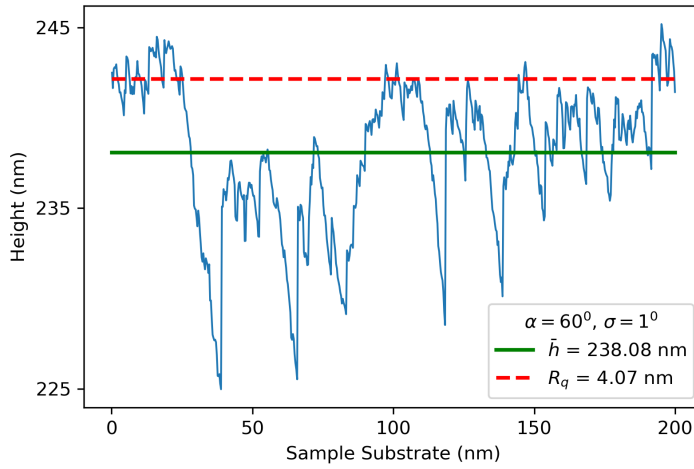


Figure 6: The surfaces of ballistic deposition thin-films appear in 2D as shown below. Here, RMS surface roughness ( $R_q$ ) of the thin-film for an angle of deposition  $60^\circ$  with the standard deviation of  $1^\circ$ .

Figure 6 shows the typical two-dimensional peaks and valleys on the surface of thin-films grown in the present simulations. To measure the RMS surface roughness ( $R_q$ ), the surface in the range of sampling length is divided into small bins whose size is equal to the size of the discs. Then mean height ( $\bar{h}$ ) and the root mean square deviation of all heights (RMS surface roughness) are measured for all the simulations carried out in the present study.

Figure 7 shows the RMS surface roughness as a function of the angle of deposition. In general, It is observed that RMS surface roughness increases with the increase in the angle of deposition for a given standard deviation. To understand the effect of standard deviation on RMS surface roughness, simulations are carried out with discs of a fixed radius equal to  $1.5\text{\AA}$  using standard deviations  $1^\circ$ ,  $2^\circ$ ,  $4^\circ$ ,  $6^\circ$  and  $10^\circ$ . It can be seen that there is no specific trend for the change in RMS surface roughness with the change in the standard deviation of the angle of deposition. To estimate the statistical error, ten simulations are carried out with  $\sigma = 1^\circ$  and the average values are plotted with their statistical error. The change in RMS surface roughness is insignificant for  $\alpha < 60^\circ$  and it is within the error-bars. Figure 7 shows that the values of RMS surface roughness range from 2-16 nm closely match with the reported range 2-14 nm from the surface analysis of OAD evaporated thin-films by atomic force microscopy (AFM) [24, 43, 44].

To understand the effect of size of the particles on RMS surface roughness, simulations are carried out with the discs of radii equal to  $1.0\text{\AA}$ ,  $1.5\text{\AA}$ ,  $2.0\text{\AA}$  and  $2.5\text{\AA}$  using a fixed standard deviation equal to  $1^\circ$  at

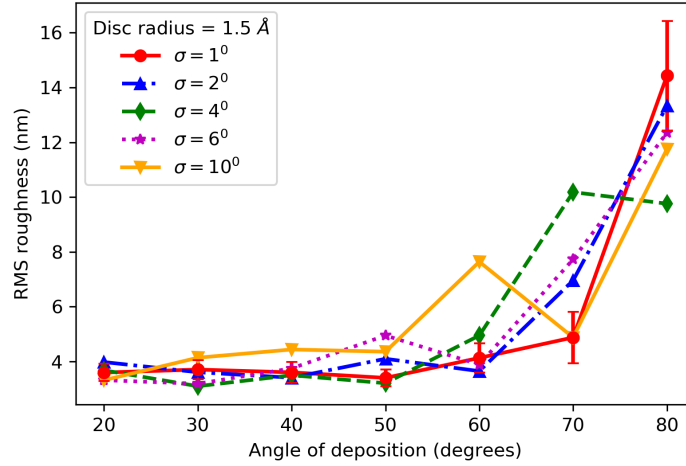


Figure 7: Variation of surface roughness as a function of angle of deposition. The roughness increases with the increase in the angle of deposition and the trend does not depend on the standard deviation used in angle of depositions

each angle of deposition. Figure 8 shows that the RMS surface roughness increases with the increase in the angle of deposition for a given size of the particles. We can also see that the RMS surface roughness increases with the increase in the size of the particles. Here, the mean values of RMS surface roughness with their statistical error are plotted for the particles of radius equal to  $1.5\text{\AA}$ .

#### 4. Application of 2D-BD to an experimental study

The collimated glancing angle deposition (C-GLAD) technique is found to be more effective than a simple GLAD for optimizing the microstructure of thin-films. In this technique, a collimator is placed parallel to the substrate at a suitable distance ( $D_{SC}$ ) as shown in Figure 9. With this, the angular spread of incoming flux can be constrained and the maximum tunability in the morphology of the deposition can be achieved. Haque et al. tailored the refractive index of silicon-dioxide thin-film using the C-GLAD technique [45]. Using this technique, they have also shown the tunability of Ag morphology [17]. They demonstrated the change in morphology of Ag deposits from a nearly continuous film with nano-columns to nano-islands of varying size with the change in the height of the substrate from its bottom edge.

Five equidistant locations on the substrate have been considered for various characterizations. Figure 9-A shows these as spots 1 & 5 ( $P_1$  and  $P_5$ ) on the substrate and the remaining spots 2–4 (or  $P_2, P_3, P_4$ ) evenly spaced in between the spots 1 & 5. It also shows the variation in constraintment of the angular spread of

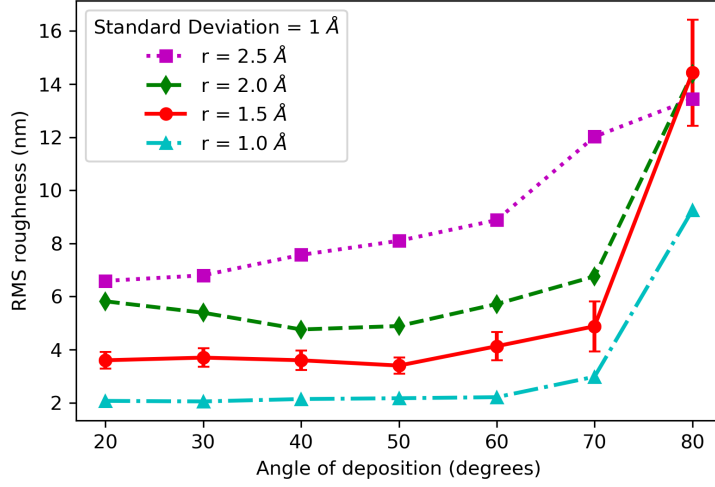


Figure 8: Variation of surface roughness as a function of size of the disc. In general, surface roughness increases with increase in the size of the particle.

the flux reaching these points. The number of atoms reaching the substrate decreases substantially with the increase in height of the substrate from its bottom edge, due to the increasing constraint on the incoming flux. In the initial phase of the thin-film growth, small stable clusters of atoms nucleate and grow into three-dimensional nano-islands. Later, these nano-islands coalesce to become a continuous, rough thin-film. At spot-1, the film is almost continuous due to larger deposition. At spot-2, it has nanorod structures with the reduced deposition. From spot-3 onwards with further reduction in the beam deposition, only discrete nano-islands form and they do not grow large enough to merge and form a continuous film within the allowed deposition time.

With the current 2D-BD, which takes into consideration only geometric effects, we performed simulations to grow films with the reported thickness mentioned in Table 1. To reproduce the features of spot-1, we need to deposit a sufficient number of discs with an angular spread of  $\theta_1$ . To do this, we deposit a sufficient number of discs at an angle of deposition  $\alpha_1 (= 90 - \frac{\theta_1}{2})$  with respect to normal of the substrate and with a standard deviation of  $\frac{\theta_1}{2}$  in the normal distribution. These angles of deposition and their standard deviations are mentioned in Table 1. This allows the incoming flux at an angle of  $\theta_1$  at the spot-1 as shown in Figure 9-B. Similarly, we carried out ballistic deposition simulations with the angles of deposition  $\alpha_2-\alpha_5$  and their standard deviations of  $\theta_2/2-\theta_5/2$  for the spots 2-5. The parameters used in these simulations are given in

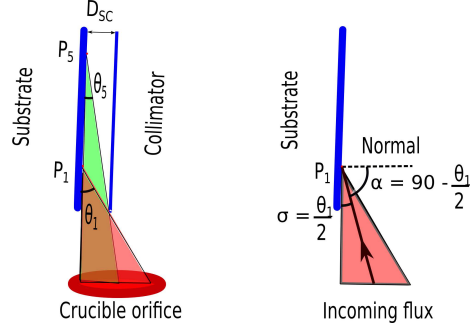


Figure 9: The schematic diagram of the collimated glancing angle deposition (C-GLAD) experiment shows the angular constraintment due to a collimator for different equidistant spots on the substrate.

Table 1.

Spot	$\alpha_n$	$\sigma_n$	Thickness
1	78.2	11.8	250 nm
2	86.2	3.8	42 nm
3	87.7	2.3	26.3 nm
4	88.4	1.6	18.4 nm
5	88.7	1.3	16.7 nm

Table 1: Parameters used to reproduce the experimental results by Haque et al. [17]. Note that the angle of deposition  $\alpha_n$  is measured from the normal to the substrate and  $\sigma_n$  is its standard deviation. Here,  $n$  takes the values from 1–5 for the spots 1–5.

The 2D-BD simulations reproduce similar structures as obtained by Haque et al. and can be seen in Figure 10. They reported a continuous thin-film of height 250 nm for the spot-1. They observed merged nanorods of size  $135 \pm 15$  nm for spot-2. From spot-3 to 5, they did not see any nucleation and growth of nanostructures and instead found isolated nano-islands of sizes  $83 \pm 10$ ,  $40 \pm 8$ ,  $26 \pm 4$  nm for spot-3 to spot-5 respectively. From Figure 10, an almost continuous thin-film is seen for spot-1, merged nanorods for spot-2 and isolated nano-islands for spot-3 to 5. Merged nanorods of size 74 nm are seen for spot-2 and nano-islands of average size 55, 30, 30 nm are seen for spots 3–5 respectively. These observed sizes are compared with the reported sizes from the C-GLAD experiment in Table 2. Porosity for the spots- 1 & 2 are estimated to be 0.79 and 0.96. RMS surface roughness of these first and second spots are 11.25 nm, 12.04 nm respectively for the sampling lengths from 0.0–200 nm. Porosity and RMS surface roughness characterizations are not considered for the other spots as they are very small individual nano-islands. The number of the individual nano-islands per one micron length for the spots 3–5 are about 12, 16, 13 and 15, 21, 18 in the 2D-BD simulations and C-GLAD respectively.

The 2D-BD simulations could qualitatively reproduce the morphology of five equidistant spots in C-

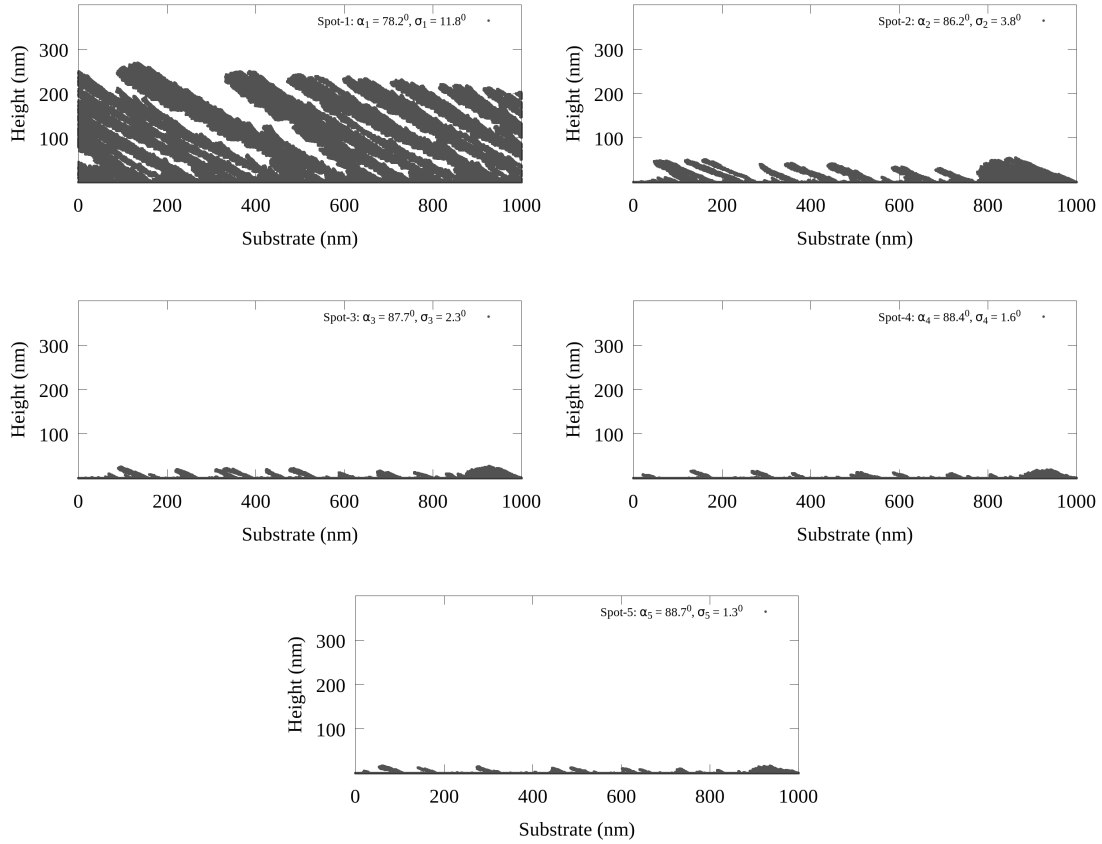


Figure 10: Nano-structures produced by 2D-BD simulations for the spots 1–5 reported by Haque et al. [17].

GLAD experiment ranging from continuous thin-film to small individual nano-islands. There is a decent quantitative match for the average sizes of the nano-structures and the average spaces between them. The values of the linear density of number of nano-islands obtained in the 2D-BD simulations for spots 3–5 are within the range of their values obtained in C-GLAD experiment. From the present study, we can realize that the results of 2D-BD simulations have a good match with the results of C-GLAD experiment.

## 5. Conclusion

A two-dimensional ballistic deposition code, “2D-BD” has been developed to study the geometric effects in ballistic deposition of thin-film growth. A total 119 2D-BD simulations have been analysed to study the morphological features such as the angle of growth ( $\beta$ ), porosity (P) and surface roughness ( $R_q$ ) as a function

Spot	Nature of the nanostructure	Average Reported size in C-GLAD	Average Observed size in 2D-BD	Average spaces between C-GLAD nanostructures	Average spaces between 2D-BD nanostructures
1	Continuous with protrusions	–	–	protrusions are contiguous	protrusions are contiguous
2	elongated nanorods	$135 \pm 15$ nm	74 nm	$53 \pm 19$	$83 \pm 16$ nm
3	isolated nano-islands	$83 \pm 10$ nm	55 nm	$44 \pm 15$	$48 \pm 15$ nm
4	isolated nano-islands	$40 \pm 8$ nm	30 nm	$33 \pm 5$	$51 \pm 27$ nm
5	isolated nano-islands	$26 \pm 4$ nm	30 nm	$35 \pm 7$	$56 \pm 19$ nm

Table 2: Comparison of sizes of nanostructures reported by Haque et al. [17] and observed in the present two dimensional ballistic deposition (2D-BD) simulations.

of angle of deposition, standard deviation in  $\sigma$  and the size of the particle. It is found that  $\beta$ ,  $P$ ,  $R_q$  increase with the increase in the angle of deposition as reported by the earlier studies. Angle of growth, porosity and RMS surface roughness do not show any significant change and definite trend with the change in the standard deviation ( $\sigma$ ) at any specific angle of deposition ( $\alpha$ ). However, few morphological changes such as thickness of the tilted columns, shape of the thin-film deposit can be observed with the change in  $\sigma$  at a given angle of deposition. The angle of growth ( $\beta$ ) remains constant with the change in size, whereas the porosity and surface roughness increase with the increase in the size of the particle. The values for angles of growth in the present study lie in between the values estimated by ‘tangent rule’ and ‘cosine rule’. These values are close to the values obtained in the experiments for pure metals and slightly far from the results for metals oxides.

2D-BD simulations are carried out to reproduce the results of collimated glancing angle deposition (C-GLAD) experiment by Haque et al. [17]. Various morphological features of the deposited films, like qualitatively matching microstructures for five equidistant spots in C-GLAD experiment ranging from continuous thin-film to small individual nano-islands are reproduced. The average sizes of nanostructures and the average spacing between them from 2D-BD simulations show a good match with the results obtained in C-GLAD experiment. The linear density of number of nano-islands obtained in 2D-BD simulations for the spots 3–5 are within the range of the values obtained in C-GLAD experiment.

## References

## References

- [1] P. M. Martin, Handbook of deposition technologies for films and coatings: science, applications and technology, 3rd Edition, William Andrew, 2010.
- [2] W. R. Grove, On the electro-chemical polarity of gases, Philosophical Transactions of the Royal Society of London (142) (1852) 87–101.
- [3] M. Faraday, X. The Bakerian Lecture.- Experimental relations of gold (and other metals) to light, Philosophical Transactions of the Royal Society of London (147) (1857) 145–181.
- [4] A. Lakhtakia, R. Messier, Sculptured thin films: Nanoengineered morphology and optics, Vol. 143, SPIE press, 2005.
- [5] D. M. Mattox, V. Mattox, Vacuum coating technology, Springer, 2003.
- [6] M. M. Hawkeye, M. T. Taschuk, M. J. Brett, Glancing angle deposition of thin films: engineering the nanoscale, John Wiley & Sons, 2014.
- [7] M. J. Vold, A numerical approach to the problem of sediment volume, Journal of colloid science 14 (2) (1959) 168–174.
- [8] D. Sutherland, Comments on Vold's simulation of floc formation, Journal of colloid science 22 (3) (1966) 300–302.
- [9] D. Henderson, M. Brodsky, P. Chaudhari, Simulation of structural anisotropy and void formation in amorphous thin films, Applied Physics Letters 25 (11) (1974) 641–643.
- [10] S. Kim, J. Henderson, P. Chaudhari, Computer simulation of amorphous thin films of hard spheres, Thin Solid Films 47 (2) (1977) 155–158.
- [11] A. Dirks, H. Leamy, Columnar microstructure in vapor-deposited thin films, Thin solid films 47 (3) (1977) 219–233.
- [12] H. Leamy, A. Dirks, Microstructure and magnetism in amorphous rare-earth–transition-metal thin films. I. Microstructure, Journal of Applied Physics 49 (6) (1978) 3430–3438.

- [13] M. Popescu, Defect formation in amorphous structures as revealed by computer simulation, *Thin Solid Films* 121 (4) (1984) 317–347.
- [14] P. Meakin, R. Jullien, Restructuring effects in the rain model for random deposition, *Journal de Physique* 48 (10) (1987) 1651–1662.
- [15] T. Mansour, R. Rastegar, A. Roitershtein, On ballistic deposition process on a strip, *Journal of statistical physics* 177 (4) (2019) 626–650.
- [16] P. Meakin, R. Jullien, Invited paper, Simple ballistic deposition models for the formation of thin films, in: *Modeling of Optical Thin Films*, Vol. 821, International Society for Optics and Photonics, 1988, pp. 45–55.
- [17] S. M. Haque, R. De, A. Mitra, J. Misal, C. Prathap, P. V. Satyam, K. D. Rao, Demonstration of tunable Ag morphology from nanocolumns to discrete nanoislands using novel angle constrained glancing angle EB evaporation technique, *Surface and Coatings Technology* 375 (2019) 363–369.
- [18] J. Nieuwenhuizen, H. Haanstra, Microfractography of thin films, *Philips Tech Rev* 27 (3) (1966) 87–91.
- [19] I. Hodgkinson, Q. hong Wu, J. Hazel, Empirical equations for the principal refractive indices and column angle of obliquely deposited films of tantalum oxide, titanium oxide, and zirconium oxide, *Applied optics* 37 (13) (1998) 2653–2659.
- [20] R. Tait, T. Smy, M. Brett, Modelling and characterization of columnar growth in evaporated films, *Thin Solid Films* 226 (2) (1993) 196–201.
- [21] Y. Zhao, Y. He, C. Brown, Composition dependent nanocolumn tilting angle during the oblique angle co-deposition, *Applied Physics Letters* 100 (3) (2012) 033106.
- [22] H. Zhu, W. Cao, G. K. Larsen, R. Toole, Y. Zhao, Tilting angle of nanocolumnar films fabricated by oblique angle deposition, *Journal of Vacuum Science & Technology B, Nanotechnology and Microelectronics: Materials, Processing, Measurement, and Phenomena* 30 (3) (2012) 030606.
- [23] G. G. Lola, J. Parra-Barranco, J. R. Sánchez-Valencia, A. Barranco, A. Borrás, A. R. González-Elipé, M.-C. García-Gutiérrez, J. J. Hernández, D. R. Rueda, T. A. Ezquerro, Correlation lengths, porosity and water adsorption in  $TiO_2$  thin films prepared by glancing angle deposition, *Nanotechnology* 23 (20) (2012) 205701.

- [24] A. Barranco, A. Borrás, A. R. González-Elípe, A. Palmero, Perspectives on oblique angle deposition of thin films: From fundamentals to devices, *Progress in Materials Science* 76 (2016) 59–153.
- [25] P. Meakin, Formation of fractal clusters and networks by irreversible diffusion-limited aggregation, *Physical Review Letters* 51 (13) (1983) 1119.
- [26] P. Meakin, The Vold-Sutherland and Eden models of cluster formation, *Journal of colloid and interface science* 96 (2) (1983) 415–424.
- [27] P. Meakin, P. Ramanlal, L. M. Sander, R. Ball, Ballistic deposition on surfaces, *Physical Review A* 34 (6) (1986) 5091.
- [28] R. Jullien, P. Meakin, Simple three-dimensional models for ballistic deposition with restructuring, *EPL (Europhysics Letters)* 4 (12) (1987) 1385.
- [29] P. Meakin, Ballistic deposition onto inclined surfaces, *Physical Review A* 38 (2) (1988) 994.
- [30] P. Meakin, *Fractals, scaling and growth far from equilibrium*, Vol. 5, Cambridge university press, 1998.
- [31] R. Jullien, P. Meakin, Computer simulations of steepest descent ballistic deposition, *Colloids and Surfaces A: Physicochemical and Engineering Aspects* 165 (1-3) (2000) 405–422.
- [32] T. Karabacak, J. Singh, Y.-P. Zhao, G.-C. Wang, T.-M. Lu, Scaling during shadowing growth of isolated nanocolumns, *Physical Review B* 68 (12) (2003) 125408.
- [33] S. Mukherjee, D. Gall, Power law scaling during physical vapor deposition under extreme shadowing conditions, *Journal of Applied Physics* 107 (8) (2010) 084301.
- [34] R. Alvarez, L. González-García, P. Romero-Gómez, V. Rico, J. Cotrino, A. R. González-Elípe, A. Palmero, Theoretical and experimental characterization of  $TiO_2$  thin films deposited at oblique angles, *Journal of Physics D: Applied Physics* 44 (38) (2011) 385302.
- [35] A. W. Sood, D. J. Poxson, F. W. Mont, S. Chhajed, J. Cho, E. F. Schubert, R. E. Welsler, N. K. Dhar, A. K. Sood, Experimental and theoretical study of the optical and electrical properties of nanostructured indium tin oxide fabricated by oblique-angle deposition, *Journal of nanoscience and nanotechnology* 12 (5) (2012) 3950–3953.

- [36] B. C. Hubartt, X. Liu, J. G. Amar, Large-scale molecular dynamics simulations of glancing angle deposition, *Journal of Applied Physics* 114 (8) (2013) 083517.
- [37] T. Ott, G. Gerlach, Morphological characterization and porosity profiles of tantalum glancing-angle-deposited thin films, *Journal of Sensors and Sensor Systems* 9 (1) (2020) 79–87.
- [38] J. Krug, P. Meakin, Microstructure and surface scaling in ballistic deposition at oblique incidence, *Physical Review A* 40 (4) (1989) 2064.
- [39] R. Tait, T. Smy, M. Brett, A ballistic deposition model for films evaporated over topography, *Thin Solid Films* 187 (2) (1990) 375–384.
- [40] K. Banerjee, J. Shamanna, S. Ray, Surface morphology of a modified ballistic deposition model, *Physical Review E* 90 (2) (2014) 022111.
- [41] B. Mal, S. Ray, J. Shamanna, Surface properties and scaling behavior of a generalized ballistic deposition model, *Physical Review E* 93 (2) (2016) 022121.
- [42] M. Backholm, M. Foss, K. Nordlund, Roughness scaling in titanium thin films: a three-dimensional molecular dynamics study of rotational and static glancing angle deposition, *Applied surface science* 268 (2013) 270–273.
- [43] Y. Luo, M. Lin, N. Zhou, H. Huang, C.-T. Tsai, L. Zhou, Molecular dynamics simulation study of the microstructure of a-Si: H thin film grown by oblique-angle deposition, *Physica B: Condensed Matter* 545 (2018) 80–85.
- [44] B. Bouaouina, C. Mastail, A. Besnard, R. Mareus, F. Nita, A. Michel, G. Abadias, Nanocolumnar tin thin film growth by oblique angle sputter-deposition: Experiments vs. simulations, *Materials & Design* 160 (2018) 338–349.
- [45] S. M. Haque, K. D. Rao, S. Tripathi, R. De, D. Shinde, J. Misal, C. Prathap, M. Kumar, T. Som, U. Deshpande, et al., Glancing angle deposition of  $SiO_2$  thin films using a novel collimated magnetron sputtering technique, *Surface and Coatings Technology* 319 (2017) 61–69.